Microstructured optical fiber sensor with three-core Mach-Zehnder interferometer

Pingsheng Xue, Qiang Wu, Yongqing Fu, Wai Pang Ng, *Senior Member, IEEE*, Richard Binns, and Qiang Liu

***Abstract*—A new type of microstructured optical fiber with a hollow channel and three cores for sensing application is designed. Fabrication method and sensing characteristics of the microstructured fiber are demonstrated. The fiber has three different kinds of cores attached on the inner wall of a capillary. One core is exposed in the capillary, another core is in an inner tube, and the last core is covered by cladding. By splicing short sections of multi-mode fiber on both ends of the microstructured fiber, these cores form a Mach-Zehnder interferometer. Light transmitted in three cores interfere with each other, as a result the spectrum consists of different interference components which can be analyzed by the Fast Fourier Transform. By extracting these components with filters, liquid refractive index and temperature sensing can be realized with sensitivities of -1319.56 nm/RIU and 0.32 nm/°C.**

***Index Terms*—Microstructured optical fiber, Mach-Zehnder interferometer, Refractive index sensing, Temperature sensing**

I. Introduction

NEW types of fibers with novel microstructures have been designed and fabricated continuously in the last 20 years, which have provided a better platform for researchers to develop new type fiber-optic sensors [1]. Microstructured optical fibers (MOF) have been developed for the needs of sensing objects to achieve optimal performance by enhancing influences of the factors on light waves. Because their sensing structures are already embedded in the fiber, it can save complicated fiber post-possessing procedures such as etching, laser drilling, tapering or film covering to some extent. MOFs with micro-channels provide a good platform for solutions to interact with light, allowing the light transmitted in the fiber to have a large overlap with the solutions so that the fiber profile can be tailored [2]. Based on this the liquid refractive index (RI) sensors are widely designed [3, 4]. In Ref. [5], a photonic crystal fiber with one-sixth of its cladding left empty forming a fluidic channel was fabricated by the stack and draw method. Therefore liquid in the channel modulates the birefringence and the fiber can be used for liquid RI sensing in a Sagnac interferometer. RI sensing and DNA detection with a tapered suspended exposed core fiber was investigated in Ref. [6]. Sensors based on MOFs have also been used in the measurement of many other parameters such as temperature [7], stress [8], chemical and biomedical detections [9, 10]. The MOFs have received extensive research interest in optical fiber sensing and further set off a new area of Lab-in-Fiber technology [11], greatly expanding the application field of optical fiber sensors.

Manuscript received ******; revised *******.This research was funded by the National Natural Science Foundation of China (Grant No. 51907017), Hebei Natural Science Foundation (Grant No. F2020501040), the Fundamental Research Funds for the Central Universities of China (Grant No. N2123012). (Corresponding author: Qiang Liu.)

Pingsheng Xue and Qiang Liu are with the College of Information Science and Engineering, Northeastern University, Shenyang 110819, China. School of Control Engineering, Northeastern University at Qinhuangdao, Qinhuangdao 066004, China and also with the Hebei Key Laboratory of Micro-Nano Precision Optical Sensing and Measurement Technology, Qinhuangdao 066004, China (e-mail: 2210386@stu.neu.edu.cn; liuqiang@neuq.edu.cn). Qiang Wu, Yongqing Fu and Wai Pang Ng are with the Faculty of Engineering and Environment, Northumbria University, Newcastle upon Tyne NE1 8ST, U.K. (e-mail: qiang.wu@northumbria.ac.uk; richard.fu@northumbria.ac.uk; wai-pang.ng@northumbria.ac.uk; richard.binns@northumbria.ac.uk)

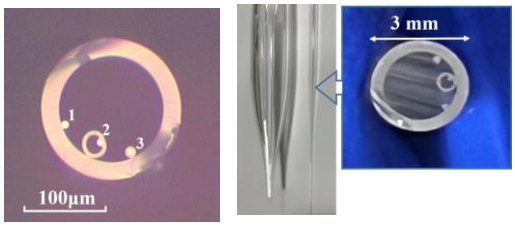

(a) (b)

Fig. 1. (a) Cross section of the fiber. The diameters of core 1 core 2 and core 3 are ~10 μm, ~8 μm and ~8 μm the cladding diameter of core 3 is ~16.5 μm. (b) Fiber preform and the cane after first drawing.

Here in this letter we propose a new type of MOF with three cores that can form a Mach-Zehnder interferometer (MZI). Three cores in the fiber are in different designing. One core is exposed and its mode effective RI is sensitive to the surrounding, which is suitable for liquid RI sensing. Another core is placed in a small channel in which can be infiltrated with other materials, for example adding temperature sensitive ones, it can respond to varying temperature. The third core is for reference. In experiment, we investigate the liquid RI and temperature sensing characteristics of the fiber. The sensing performance and potential application of the fiber are also discussed.

II. Fiber fabrication and principle

The fiber is hollow and has three cores attached on the inner wall (Fig. 1(a)). There is no cladding surrounding core 1 and core 2. Core 1 is exposed but core 2 is suspended

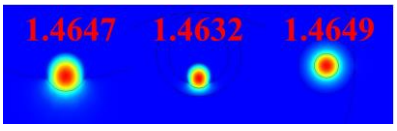

Fig. 2. Mode profile and calculated mode effective RI.

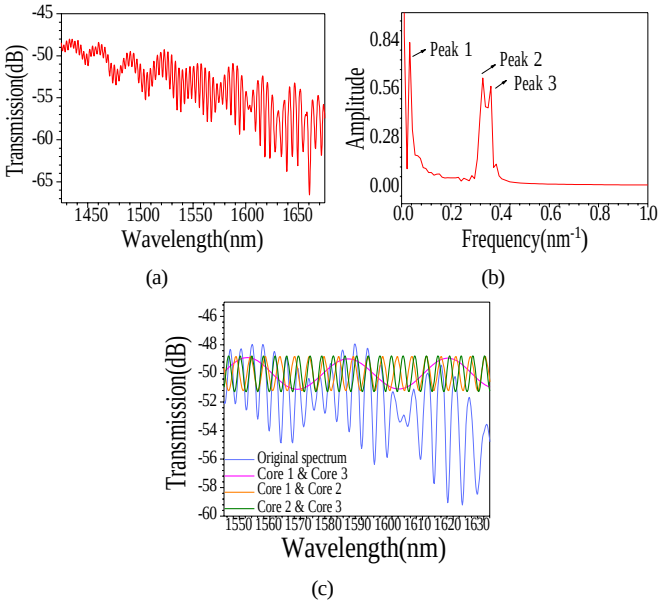

Fig. 3. (a) Output spectrum of the MZI with the fiber. (b) FFT of the output spectrum, three peaks indicate three interference components. (c) Each component: interference 1&3, 1&2, and 2&3 filtered from original spectrum.

in an inner tube. The tubes and cladding of the fiber are made of pure silica. The cores are slica doped with Ge which slightly increased the RI than pure silica. The RIs of core 1 and core 2 are ~1.465. The RI of core 3 is ~1.47 and it is surrounded by silica cladding. The fabrication procedures of the fiber preform are as follows. Two core rods without claddings (diameters 1.2 mm and 1.5 mm), a cladding-covered core rod (core/cladding diameters 1 mm/2.3 mm) and a thin silica tube were assembled in an outer tube whose diameter is 14 mm/20 mm (inner/outer) according to the fiber structure. Then the tube was scanned with oxy-hydrogen torch, the rods and thin tube were slightly softened and adhered to the inner wall. Their arrangements were fixed before drawing on a fiber drawing tower. The preform was firstly drawn into canes with a diameter of ~3 mm, and then the canes were drawn again into final fibers with a diameter of ~165 μm. In the finished fiber, core 1 and core 2 are ~10 μm and

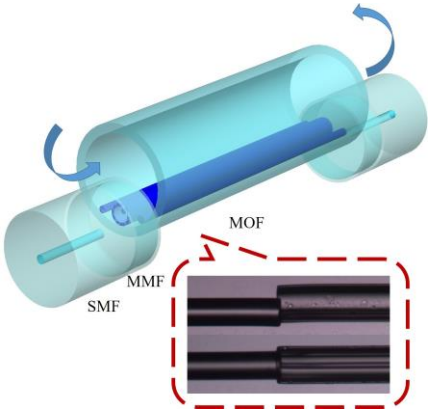

Fig. 4. Schematic of the fiber splicing. Eccentric splicing creates entrance and exit for fluids. (Inset: Side and top views of the splicing point.)

~8 μm in diameters respectively, and core 3 is ~8 μm/16.5 μm (core/cladding). The distances between adjacent cores are ~40 μm, so the waveguide coupling between cores are negligible. The cladding of core 3 is thick enough so that its mode effective RI is not influenced by the surrounding RI in the capillary. The two step drawing technique can maintain the good shape of the microstructure, preventing the inner channel collapsed and the core deformed [12]. Fig. 1(b) shows the preform and cane after drawing. The fundamental mode profiles of the three cores are shown in Fig. 2. The finite element simulations by Comsol 5.6 show the mode effective RI of core 3 is the highest. Core 1 is slightly lower than core 3, while core 2 is the lowest. The simulations only provide a reference, comparing mode effective RIs among the three cores. The exact mode effective indices are not so precise because the RI of material may change slightly during thermal drawing [13].

The three core microstructured fiber can form an MZI by splicing with two short sections of 105/125 multi-mode fiber (MMF) on both ends. The lengths of MMF should be as short as possible so that the phase differences between guided modes in MMF can be negligible. Light is incident into all three cores due to the large core of MMF. Phase differences generates and interferences occurs after transmitting in the MOF. Considering the fundamental modes of three cores which have the highest intensities only, light in every two cores interferes with each other so there are mainly three interference components. The output spectrum is the sum of these three interferences, and the output intensity can be expressed as [16]:

$$\begin{aligned} I = 2(I_1 + I_2 + I_3 &+ 2\sqrt{I_1 I_2}\cos\varphi_{12} \\ &+ 2\sqrt{I_2 I_3}\cos\varphi_{23} \\ &+ 2\sqrt{I_1 I_3}\cos\varphi_{13}) \end{aligned}$$

where I_1, I_2 and I_3 are intensities in each core, φ_{12}, φ_{23} and φ_{13} are phase differences between each two cores, $\varphi = 2\pi\Delta nL/\lambda$, Δn is mode effective RI differences between cores, L is the fiber length. Connected with a supercontinuum light source (470-2400 nm, SC-5, YSL) whose coherence length is over 2 mm and an optical spectrum analyzer (OSA) (AQ6370D, Yokogawa), the output spectrum can be obtained and is plotted in Fig. 3(a). The length of the fiber is 20 cm. The spectrum consists of multiple interference dips. The small free spectrum ranges (FSRs) of the dense dips are ~3 nm, and the large FSRs are ~30 nm. The resolution of the OSA is 0.5 nm so the noise sampled is very low while the small dips can still be distinguished. An over long fiber may result in exceeding the coherence length between the cores, then the dense dips cannot be observed. A shorter fiber will result in large FSRs, it cannot form envelope perfectly in the wavelenghths we observe. Moreover the intensities of high order modes are high which impair the interference spectrum if the fiber is too short. Approximately 20 cm is the most suitable length. If we perform the Fast Fourier Transform (FFT) to the spectrum, three main peaks are obtained, indicating that the spectrum contains three interference components (Fig. 3(b)). Peak 1 has the lowest frequency, and it is much lower than other two peaks. It corresponds to the interference between core 1 and core 3 (1&3). This is because their mode effective

indices are close, according to the FSR estimating equation: $FSR = \lambda^2/\Delta nL$, it results in the largest FSR. Similarly, we may conclude peak 2 corresponds to interference between core 1 and core 2 (1&2), peak 3 correspond to interference between core 2 and core 3 (2&3). Because the FSR tends to increase with wavelength, the FFT cannot be performed in very wide wavelength range, usually a span within 100 nm is considered, and the sampling interval is 0.2, then each main peak can be distinguished. Each interference component can be extracted by FFT filters with narrow passbands (0.01 nm^{-1} bandwidth) according to the peak frequencies, which are related with the wavelength range and FSRs. Fig. 3(c) shows each component in wavelength span 1540~1640 nm extracted by filters with passbands of 0.027~0.037, 0.205~0.215 and 0.260~0.270 and the sum of them makes up the original spectrum.

III. Experiment Results and Discussion

Because the cores are attached on the inner wall of the capillary, to incident light into all the three cores, the splicing with MMF is eccentric. This creates entrance and exit for fluids at the ends of the fiber. The ends of the inner channel were sealed after splicing. Fig. 4 shows the schematic of the design. The splicing can be realized by a polarization maintaining fiber splicer (FSM-100P+, Fujikura), which is able to observe and rotate the fiber end face as well as set an offset aligning in splicing procedure. The splicing discharge intensity is low and discharge duration is short to prevent the fiber collapse. 4~6 times of additional discharge will improve the the strength of the splicing point. The fluids infiltrated into the fiber will directly influence the mode effective RI of core 1 which is exposed. However core 2 and 3 are insensitive to the fluids because core 2 is isolated in the inner channel and core 3 is covered by cladding. The fiber has the potential to be applied as a liquid RI sensor. Thus the characteristics for liquid RI sensing of the fiber was investigated. 20 cm of the fiber was used to form the MZI and then put in a cell which was filled with NaCl solution. The solution filled the fiber main channel through capillary effect in 20 seconds. The depth of the liquid solution was shallow so the pressure can be neglected. The solution RI was adjusted by the NaCl concentration. The RIs of different concentration of NaCl solution were given by a refractometer (PAL-RI, Atago). The interferences 1&3 and 1&2 were influenced by the solution RI. In experiment, it took about 40 minutes for the spectrum to stabilize as the liquid RI increase or decrease to a new value. The spectra obtained when the fiber was in different RI solutions are shown in Fig. 5(a). To have a clear view, the interferences among three cores were extracted by filter. As the RI of solution rises, the mode effective RI of core 1 increases while core 3 is unchanged, decreasing the phase differences between core 1 and core 3 so the interference spectrum shifts to short wavelength (Fig. 5(b)). Conversely, the phase difference between core 1 and core 2 increases with the increasing RI, causing red shift of the interference spectrum (Fig. 5(c(i))). The interference spectrum between core 2 and 3 hardly shift because neither core 2 nor core 3 can be influenced by the infiltrated liquid (Fig. 5(c(ii))). Liquid RI sensing can be realized by observing

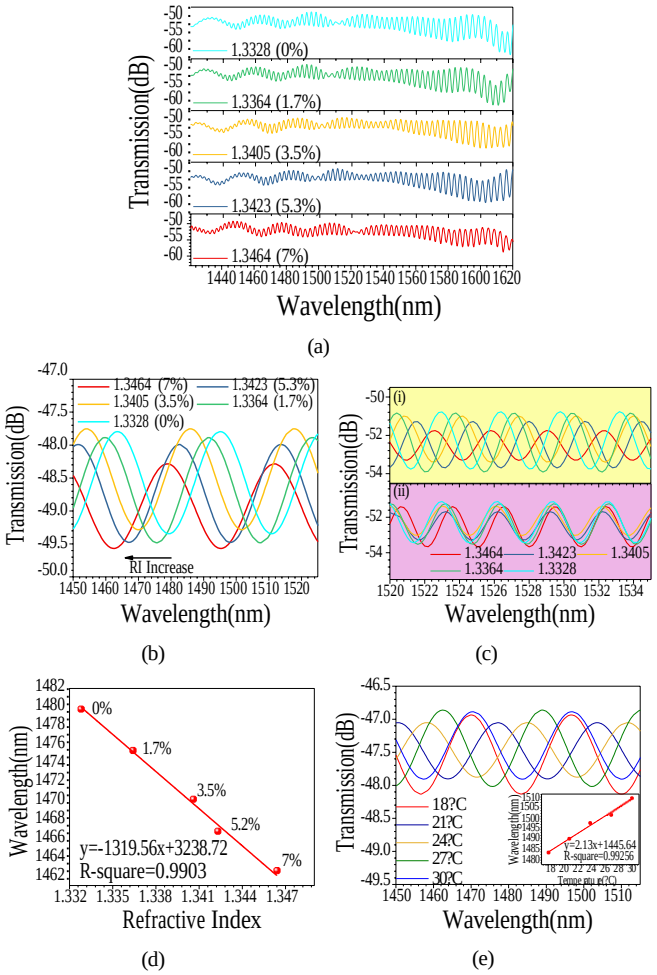

Fig. 5. (a) Spectrum of the MZI when the fiber is in different concentration/RI of NaCl solutions. (b) Interferences of (i) core 2&3 and (ii) core 1&2. (d) Linear fitting of dip wavelength shift of interference core 1&3. (e) Wavelength shift of interference core 1&3 caused by temperature (inset: linear fitting of the wavelength shift, indicated the temperature cross sensitivity is 2.13 nm/°C)

the wavelength shift of the interference 1&3. The shift of dip wavelength is plotted in Fig. 5(d). The slope of linear fitting result indicates that the RI sensitivity is -1319.56 nm/RIU for NaCl solution. The influence of temperature was also considered. The interference spectrum between core 1 and core 3 red shifted with increasing temperature obviously (Fig. 5(e)). That means the influence of temperature is not negligible and need to be compensated during RI sensing, which will be discussed later.

Temperature sensing is another ability of the fiber. The inner channel can be infiltrated with high thermal-optical coefficient materials, which modulate the mode effective RI of core 2. The RI of infiltrated material should be lower than that of the core, ensuring the light is guided in the core by the index guiding mechanism. In experiments, ethanol was infiltrated in the inner channel before splicing. Although all three interferences are influenced by temperature to a certain extent because of the uneven thermal expansion or internal strain due to its special asymmetry structure, the interferences related with core 2 are more concerned because of the infiltrated ethanol. The superposition of interferences 1&2 and 2&3 forms envelopes.

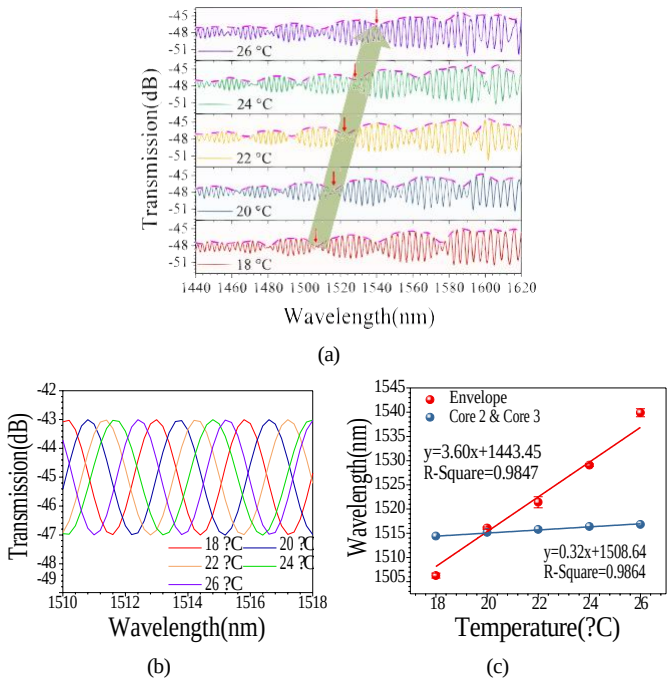

Fig. 6. (a) The spectra composed of interferences 1&2 and 2&3 at different temperatures, interference 1&3 is filtered out. The dash curves are outlines of the upper envelopes. (b) Interference between core 2 and core 3, it is related with temperature only and cannot be influenced by the RI in main channel. (c) Wavelength shifts of the envelope dip and interference 2&3 with temperature.

When temperature rises, the RI of ethanol decreases, which causes the decrease of effective RI of core 2. Fig. 6(a) shows the spectra from 18 ℃ to 26 ℃ without the interference 1&3. The spectrum red shifts with increasing temperature. The dash curve outlined the upper envelope and the wavelength shift of one of its dip is shown in Fig. 6(c). The interference 2&3 was further filtered out to consider separately. Fig. 6(b) shows the spectrum of the interference 2&3 (normalized, for easier observation) at different temperatures. Increased temperature caused more phase difference between core 2 and core 3 and resulted in red shift of the dips. The wavelength shifts are plotted in Fig. 6(c).The advantage of extracting the interference 2&3 from the original spectrum is that it responds to temperature only and is independent from the RI in main channel because core 2 and core 3 are insensitive to the surrounding, and we may use this to compensate the influence of temperature in RI sensing.

The fiber has shown the potentials to be used as liquid RI and temperature sensors. The responses can be considered linear. By extracting the interference 2&3 which is irrelevant with solution RI, temperature sensing can be realized and then we can compensate the influence of temperature in RI sensing which is realized by extracting interference 1&3. The wavelength shift caused by RI varying is: $\Delta\lambda_{RI}^{1,3} = \Delta\lambda^{1,3} - 2.13\Delta T$. Other than that, single parameter temperature sensing can be realized with a higher sensitivity which reached 3.6 nm/℃ by tracking the envelope composed by interferences 1&2 and 2&3. The experiment was carried out in a cell. When there were disturbances such as water flowing or even stirring, the spectrum was very stable if the fiber had been fixed properly and it worked stably during a long time.

IV. Conclusion

A three cores MOF was proposed, it formed a MZI and the sensing characteristics of the fiber was investigated. Liquid RI and temperature sensing was achieved by extracting different interference components from the spectra. Single parameter of temperature sensing sensitivity can be improved by tracking the envelope composed by two interference components. Although the sensitivity may not as high as fiber sensors based on other principles such as SPR or waveguide coupling, the microstructured fiber can be drawn very long. It is easily realize mass production which is an advantage in cost saving and productization. The sensing device shows good stability in experiment. The RI and temperature sensor based on this fiber can be applied in harsh situations like water treatment industry or maritime monitoring. The fiber is also possible to be used in microfluidic for broader applications such as biochemical sensing and lab-in-fiber or lab-on-a-chip.

References

[1] P. Xue, Q. Liu, S. Lu, Y. Xia, Q. Wu and Y. Fu, A review of microstructured optical fibers for sensing applications, Opt. Fiber Technol., vol 77, 2023.

[2] T. Yuan, X. Zhang, Q. Xia, Y. Wang and L. Yuan, Design and fabrication of a functional fiber for micro flow sensing, IEEE J. Lightwave Technol., vol. 39, no. 1, pp. 290-294, 2021.

[3] S. Xu, W. Chang, Y. Luo, W. Ni, Y. Zheng, L. Wei, Z. Xu, Z. Lian, Y. Zhang, Y. Huang and P. Shum, Ultrasensitive Broadband Refractometer Based on Single Stress-Applying Fiber at Dispersion Turning Point, IEEE J. Lightwave Technol. vol. 39, no. 8, pp. 2528-2535, 2021.

[4] Z. Liu, X. Yang, Y. Zhang, Y. Zhang, Z. Zhu, X. Yang, J. Zhang, J. Yang and L. Yuan, Hollow fiber SPR sensor available for microfluidic chip, Sens. Actuators B Chem. Vol. 265, pp. 211-216, 2018.

[5] N. Zhang, K. Li, Y. Cui Z. Wu, P. Shum, J. Auguste, X. Dinh, G. Humbert and L. Wei, Ultra-sensitive chemical and biological analysis via specialty fibers with built-in microstructured optofluidic channels, Lab Chip, vol. 18, 655, 2018.

[6] X. Li, N. Chen, X. Zhou, Y. Zhang, Y. Zhao, L. Nguyen, H. Ebendorff-Heidepriem and S. Warren-Smith, In-situ DNA detection with an interferometric-type optical sensor based on tapered exposed core microstructured optical fiber, Sens. Actuators B Chem. 351, 130942, 2022.

[7] Y. Liang, H. Zhang, B. Huang, B. Liu, W. Lin, J. Sun and D. Wang, Ultrahigh-sensitivity temperature sensor based on resonance coupling in liquid-infiltrated side-hole microstructured optical fibers, Sens. Actuator A Phys. vol. 334, 113358, 2022.

[8] Z. Liu, C. Wu, M. Tse, and H. Tam, Fabrication, Characterization, and sensing, applications of a high-birefringence, suspended-core fiber, IEEE J. Lightwave Technol. vol. 32, no. 11, pp. 2113-2122, 2014.

[9] A. Zhang, Z. Liu, Q. Tu, Q. Ma, H. Zeng, Z. Deng R. Jiang, Z. Mo, J. Liu, C. Xia, N. Zhao, Z. Hou, X. Huang and G. Zhou, Trace detection of cadmium (II) ions based on an air-hole-assisted multicore microstructured optical fiber, Sens. Actuators B Chem., vol. 365, 131941, 2022.

[10] X. Li, N. Chen, X. Zhou, Y. Zhang, Y. Zhao, L. Nguyen, H. Ebendorff-Heidepriem and S. Warren-Smith, In-situ DNA detection with an interferometric-type optical sensor based on tapered exposed core microstructured optical fiber, Sens. Actuators B Chem., vol. 351, 1309422, 2022.

[11] S. Pissadakis, Lab-in-a-fiber sensors: A review, Microelectron. Eng., 217, 111105, 2019.

[12] M. Tse, Z. Liu, L. Cho, C. Lu, P. Wai, and H. Tam, Superlattice microstructured optical fiber, Materials (Basel), vol. 7, no. 6, pp.4567-4573. 2014.

[13] Y. Jaluria. Manufacture of Optical Fibers: Drawing and Coating Processes. In: Advanced Materials Processing and Manufacturing. Mechanical Engineering Series. Springer, Cham. 2018.

[14] P. Xue, Q. Liu, Q. Wu and Y. Fu, The Fabrication of an Eccentric Three-Core Fiber and Its Application as a Twist Sensor, IEEE T. Instrum. Meas., vol. 71, pp. 1-6, 2022.